Journal of Physical Chemistry & Biophysics

Pavankumar et al., J Phys Chem Biophys 2014, 4:6
DOI: 10.4172/2161-0398.1000163

Research Article Open Access

Comprehensive Comparative Study Using Ab Initio Computational Approaches on the Structures of Cisplatin, Oxaliplatin and BNP3029 (A Novel Substituted Cyano Ligand-based Platinum Analogue) and Activation Energy Barriers for the Attack of Nucleophiles on Cisplatin and BNP3029 and their Monoaquated Derivatives#

Pavankumar PNV, Ayala PY, Parker AR, Zhao M, Jair K, Chen X, Kochat H and Hausheer FH*
BioNumerik Pharmaceuticals, Inc., 8122 Datapoint Drive, Suite 1250, San Antonio, TX 78229, USA

Abstract

Cisplatin is an important anti-cancer agent widely used in the clinic; however, it has several notable limitations. To develop novel platinum analogues, key characteristics were considered that may result in more effective platinum analogues. Herein results based on *ab initio* geometry optimizations (gas- and solution-phase) on cisplatin (1), oxaliplatin_1R_2R (2) and BNP3029 (3, a novel substituted cyano ligand-based platinum analogue, $PtCl_2[N{\equiv}C(CH_2)_3(C_6H_5)]_2$) using the recently published potentials and basis sets for platinum are presented. Optimized quantum mechanical derived geometries of the 3 platinum agents were in good agreement with available experimental geometries. The reactivity of BNP3029 was compared to cisplatin by computing the activation free energy barriers for the attack of various nucleophiles on both 1 and 3 and their monoaquated derivatives. Based on the activation energy barriers, it was determined that: (i) the reaction rate may be similar for the attack of water on cisplatin and BNP3029; (ii) the reaction rate for the attack of DNA bases was slower for monoaquated BNP3029 compared to monoaquated cisplatin; and (iii) the reaction rates for a thiol/thiolate attack on monoaquated cisplatin or monoaquated BN3029 were similar.

BNP3029 demonstrated potent cytotoxic activity in a variety of human cancer cell lines in comparison to cisplatin and oxaliplatin and also had potent cytotoxic activity in several platinum resistant cell lines.

Keywords: Cisplatin; Oxaliplatin; BNP3029; Anti-cancer agents

Introduction

Cisplatin has been an important anticancer agent and has demonstrated a broad spectrum of anti-cancer activity against a variety of tumors including germ cell tumors, ovarian and bladder carcinomas, squamous cell tumors of the head and neck, esophageal cancers, and non-small cell lung tumors either as a single agent or in combination with other chemotherapy drugs (Figure 1) [1-3]. Despite its success as an important anti-cancer agent, cisplatin does have severe limitations in its use such as nephrotoxicity, neurotoxicity, nausea, ototoxicity and resistance to treatment over time [1]. In order to overcome these limitations, newer analogues of platinum have been developed, such as carboplatin and oxaliplatin [4] (Figure 1), but their use is limited compared to cisplatin or is a tradeoff of different serious toxicities (e.g., thrombocytopenia for carboplatin). Nedaplatin (approved only in Japan for esophageal cancer), Heptaplatin (approved in South Korea for gastric cancer) and Lobaplatin (approved in China for bladder cancer) are some of the other platinum analogues currently used in a limited country-specific manner, but these other platinum agents are not approved for use in most countries [3] (Figure1). Multinuclear platinum analogues, notably BBR3464, have been evaluated in clinical trials but did not, ultimately, gain approval [3]. Since the discovery of cisplatin's anti-tumor properties, hundreds of platinum analogues have been synthesized and tested for their anti-tumor properties and only very few have been approved for use in patients [3,5]. Newer analogues such as Picoplatin and Satraplatin [6] {a Pt (IV) analogue and also the first oral platinum agent} are currently in clinical trials (Figure 1).

Intracellularly, the postulated mechanism of action of cisplatin involves the initial replacement of one of the two chlorine atoms in cisplatin by water resulting in the formation of a reactive monoaquo-monochloro species [3]. This reactive monoaquo species attacks the exposed imidazole N7 of guanine on DNA, initially yielding a mono-platinum-DNA adduct. Once this platinum-DNA adduct is formed, the second chlorine atom on cisplatin may undergo aquation. Then, this species or the native form attacks N7 on an adjacent guanine thereby forming a majority proportion of 1,2-GG intrastrand adducts with DNA. In the majority of cases, cisplatin forms an intrastrand DNA adduct, and has a well documented selectivity for adjacent GG dinucleotide sequences [1]. 1, 2-intrastrand adducts of cisplatin with DNA are also known with adjacent AG dinucleotides but not with GA dinucleotides [1]. A minor category of cisplatin DNA adducts are due to the formation of 1,3-intrastrand (GXG, 10%, X= any nucleotide) and 1,2-interstrand (<2%) crosslinks. All of these platinum-DNA adducts have the potential to be cytotoxic and/or induce apoptosis by

***Corresponding author:** Hausheer FH, BioNumerik Pharmaceuticals, Inc., 8122 Datapoint Drive, Suite 1250, San Antonio, TX 78229,USA, Tel: 210-614-1701; Fax: 210-614-0643; E-mail: fred.hausheer@bnpi.com

Received: June 28, 2014; **Accepted:** October 15, 2014; **Published:** October 17, 2014

Citation: Pavankumar PNV, Ayala PY, (2014) Comprehensive Comparative Study Using Ab Initio Computational Approaches on the Structures of Cisplatin, Oxaliplatin and BNP3029 (A Novel Substituted Cyano Ligand-based Platinum Analogue) and Activation Energy Barriers for the Attack of Nucleophiles on Cisplatin and BNP3029 and their Monoaquated Derivatives#. J Phys Chem Biophys 4: 163. doi: 10.4172/2161-0398.1000163

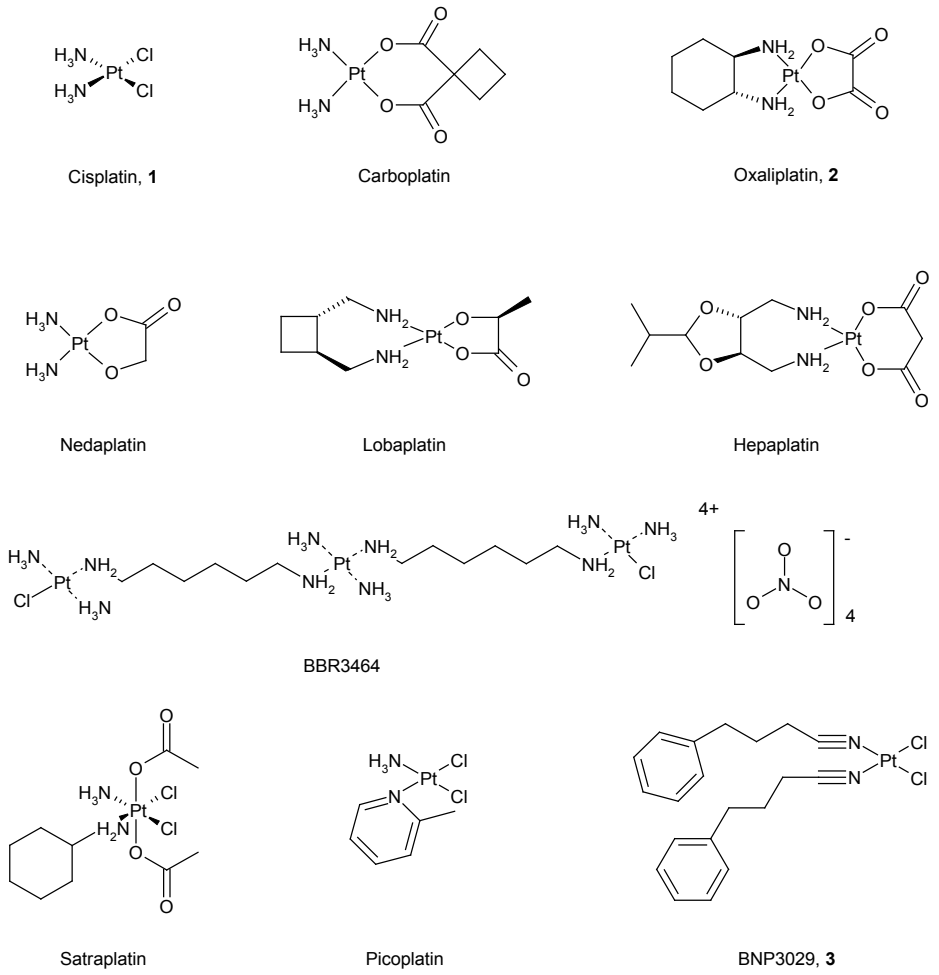

Figure 1: Structures of some platinum complexes.

the inhibition/modulation of multiple intracellular pathways important for cell growth, cell division and cell survival, including replication and transcription.

Cisplatin is an important anti-cancer agent; however, some patients develop resistance to cisplatin and the potential nephrotoxic and neurotoxic side effects also have to be carefully managed in the clinical setting [1]. In order to develop novel platinum analogues, key characteristics were considered that may result in more effective platinum analogues, such as: (a) reduced reactivity towards aquation; (b) reduced reactivity towards thiol or thiolate attack; and (c) reduction in excision repair of platinum-DNA lesions by NER proteins by maintaining a normal DNA form (B-DNA). Accordingly, we synthesized a series of platinum analogues with substituted cyano group as the carrier ligand [7] and herein describe computational studies on BNP3029 (Figure 1), a representative substituted cyano ligand-based novel platinum complex. There have been several computational studies on (a) structural properties of cisplatin and analogues [8-10]; (b) aquation of cisplatin and analogues [11-14]; (c) the base preferences of cisplatin and simulation studies on platinum-DNA adducts [15-18]; and (d) the attack of thiol/thiolate on cisplatin [19-21] and where applicable we compare this historical data with our current data.

In this paper, we describe a comprehensive comparative computational study on the structure and reactivity of cisplatin, oxaliplatin, and BNP3029 using the recently published effective core potentials and basis sets for platinum. Differences in the reactivity of cisplatin and BNP3029, and their monoaquated derivatives, with respect to nucleophilic attack by water, guanine, adenine, thiolate ($^{-}SCH_3$), and thiol ($HSCH_3$) are also evaluated herein by comparing the activation free energy barriers for these reactions.

Materials and Methods

MCF7/WT cells (human breast cancer), MCF7/ADR (adriamycin resistant MCF7 human breast cancer), A2780 cells (human ovarian cancer), A2780/CP3 cells (cisplatin resistant human ovarian cancer), A2780/C25 cells (oxaliplatin resistant human ovarian cancer) and HCT8/WT cells (human colon cancer) that were gifts from Dr. Y. Rustum of Roswell Park Cancer Institute (RPCI). MCF7-MR cells were a gift from Dr. W. Dalton at Moffit Cancer Center. MCF7/OxR cells (oxaliplatin resistant human breast cancer) and HCT-8/CisR cells (cisplatin resistant colon cancer cells) were developed at BioNumerik Pharmaceuticals, Inc. GLC/WT (human small cell lung cancer) and GLC/ADR cells (Adriamycin resistant human small cell lung cancer) were a gift from Dr. EGE de Vries and Dr. C. Meijer of the University Medical Center Groningen, Netherlands. SW480 cells (human colon cancer), CAMA-1 cells (human breast cancer), NCI-H23 cells

(human lung cancer), and NCI-H838 cells (human lung cancer) were purchased from American Type Culture Collection (ATCC). NCI-H23 and NCI-H838 were developed in the laboratory of Dr. Herbert Oie and were used pursuant to a license obtained from the Public Health Service/National Institutes of Health.

Computational Methods

The computational studies described herein were performed in using the Gaussian 03 program [22] with the density functional theory.

Cell Culture and Cytotoxicity Methods

Population doubling time for each of the cell lines used herein varied, but experiments encompassed four to five total cell doublings corresponding to approximately 4 days for HCT-8 and HCT8/CisR; 6 days for SW480; 5 days for MCF7/WT, MCF7/MR, MCF7/ADR, MCF7/OxR, A2780/WT, A2780/CP3, A2780/C25, GCL/WT and GCL/ADR; 6 days for CAMA-1; and 7 days for NCI-H838, and NCI-H23. Exponentially growing cells were seeded in 96 well microtiter plates (number of cells/well shown parenthetically) as follows: MCR7/WT (600), MCR7/ADR (1500), MCR7/MR (1500), MCF7/OxR (600), A2780/WT (500), A2780/CP3 (1000), A2780/C25 (1000), NCI-H23 (600), NCI-H838 (600), GLC/WT (500), GLC/ADR (500), HCT8 (800), HCT8CisR (1200), and CAMA-1 (800) (100 µL seeding volume). Cells were allowed to attach to microtiter plates in CO_2 incubators at 37°C overnight prior to drug treatment. Cells were treated with cisplatin, BNP3029, and oxaliplatin for 1 hour at 37C. Following drug exposure, medium was removed; cells were washed once with medium and incubated in drug-free medium for four to five cell doublings. After a total of four to five cell doublings, cell survival was evaluated using the Sulforhodamine B (SRB) assay [23].

Electronic Structure Calculations

Ab Initio optimizations (geometries and transition states) were performed using Gaussian 03 program [22] with the density functional theory [24]. The exchange-correlation functional *mPW1PW* (exchange component of Perdew-Wang as modified by Barone and correlation functional by Perdew-Wang) was employed [25]. Dunning's correlation consistent valence double-zeta cc-pVDZ basis set for the ligands such as NH_3, Cl, OH_2, $N{\equiv}C(CH_2)_3(C_6H_5)$, oxalate and 1,2-DACH (1,2-diaminocyclohexane) was used [26]. Newest energy-consistent pseudopotentials and correlation consistent basis set for the 5*d* element (Pt) from Stoll et al. [27] were employed. Six Cartesian d functions for polarization were used in all of our geometry optimizations and energy evaluations. Transition states were verified using vibrational frequency calculations (one imaginary frequency). Thermal corrections to the free energies were obtained from frequency calculations at 25°C and 1 atm. When comparing the calculated activation energy barriers with experimental data, the calculated energy barriers were corrected for liquid-phase concentrations of 1 mol/L by subtracting 1.9 kcal/mol from the calculated activation energy barriers (correction factor is: RT ln(24.46) = 1.9 kcal/mol where T = 298 K; 24.46 is the volume occupied by 1 mole of gas at 298 K) [28].

Cisplatin	Pt-Cl	Pt-N	N-Pt-N	N-Pt-Cl	Cl-Pt-Cl
Calculated	2.292 **2.340**	2.077 **2.037**	98.4 **90.5**	83.1 **88.4**	95.4 **92.7**
Expt (averaged)[1]	2.330	2.010	87.0	90.3	91.9
Expt (range)[1]	2.333, 2.328	1.950, 2.050	87.0 ± 1.5	92.0 ± 1, 88.5 ± 1	91.9 ± 0.3

[1]See reference [30]

Table 1: Gas-phase and solution-phase (bold) optimized geometries of cisplatin and the comparison of the geometries from experiment. All distances are in Å and angles are in °.

Activation Free Energy Barrier Calculation

The following equations (eqs. 1-5) were used to compute the activation free energy barriers for the attack of various nucleophiles on cisplatin and BNP3029 and their monoaquated derivatives. The activation free energy barrier was the energy difference between the transition state (TS) and the reactants in each equation. Using the gas-phase optimized geometries for each of the reactant and the TS, single point energies were obtained with the inclusion of solvent and employing the same basis sets and potentials used in the gas-phase optimizations. The solution energies for each reactant and TS were obtained by adding the *Total free energy in solution* with all non electrostatic terms and *Total non electrostatic* terms. To this sum, we added the thermal corrections to the free energy (obtained using the frequency option from the gas-phase calculation). The solvent effects were added using the polarizable continuum model (PCM) within the integral equation formalism (IEF-PCM) [29] using the Pauling radii.

$$PtL_2Cl_2 + H_2O \rightarrow \quad PtL_2Cl_2(H_2O) \qquad (1)$$

L= NH_3 (1a), $((C_6H_5)(CH_2)_3C{\equiv}N)$ (3a)

$$PtL_2Cl(OH_2)^{1+} + \text{guanine} \rightarrow \quad PtL_2Cl(\text{guanine})(H_2O)^{1+} \qquad (2)$$

L= NH_3 (1b), $((C_6H_5)(CH_2)_3C{\equiv}N)$ (3b)

$$PtL_2Cl(OH_2)^{1+} + \text{adenine} \rightarrow \quad PtL_2Cl(\text{adenine})(H_2O)^{1+} \qquad (3)$$

L= NH_3 (1c), $((C_6H_5)(CH_2)_3C{\equiv}N)$ (3c)

$$PtL_2Cl(OH_2)^{1+} + SHCH_3 \rightarrow \quad PtL_2Cl(SHCH_3)(H_2O)^{1+} \qquad (4)$$

L= NH_3 (1d), $((C_6H_5)(CH_2)_3C{\equiv}N)$ (3d)

$$PtL_2Cl(OH_2)^{1+} + SCH_3^- \rightarrow PtL_2Cl(SCH_3)(H_2O) \qquad (5)$$

L= NH_3 (1e), $((C_6H_5)(CH_2)_3C{\equiv}N)$ (3e)

Results

Several studies have been reported on the optimized geometries of cisplatin using a variety of methods, basis sets and potentials with recommendations on how to treat cisplatin computationally [10]. As far as we can ascertain, none of these aforementioned studies employed the newest platinum basis set and effective core potential reported recently [27]. Here we employed the newest basis set and potential from Stoll's group for platinum along with the recommended cc-pVDZ basis set on the ligand atoms within the density functional formalism for the geometry optimizations of cisplatin, oxaliplatin and BNP3029 to assess the performance of the new basis set and potential for platinum. Using the gas-phase optimized geometries, we also performed solution-phase optimizations of cisplatin, oxaliplatin and BNP3029 using the same basis sets and the potentials employed in the gas-phase optimizations and compared the gas-phase and solution-phase geometries to the experiment, where available (see details in sections 7.1 to 7.3).

Optimized geometries of Cisplatin

The gas-phase optimized geometries of cisplatin at the mPW1PW/cc-pVDZ basis set for Cl, and NH_3 and the platinum basis set and potential from Stoll's group [27] are shown in Table 1 and Figure 2A. The gas-phase optimized geometry indicated that the Pt-Cl bond length (2.292 Å) was shorter than the experimental value (2.330 Å) whereas the Pt-N bond length (2.077 Å) was longer than the experimental value (2.010 Å). Inclusion of solvent corrected these anomalies with both Pt-Cl (2.340 Å) and Pt-N (2.037 Å) bond lengths agreeing very well with the experimental values [30].

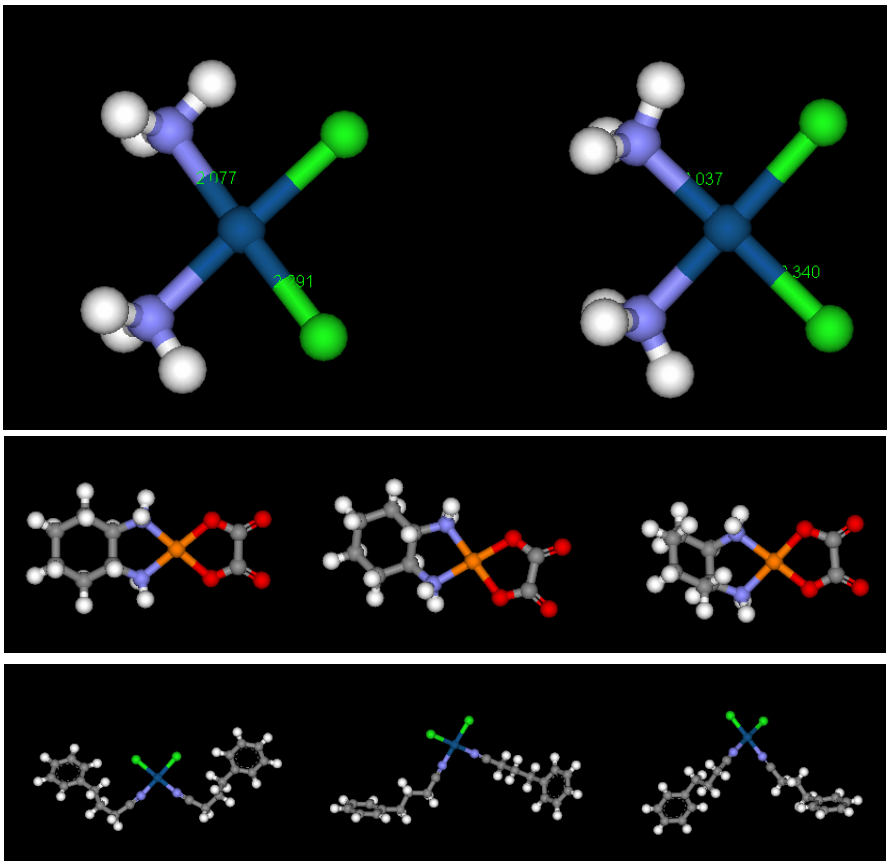

Figure 2: Optimized structures of A) Cisplatin. Left: gas-phase optimized geometry and Right: Solvent-phase optimized geometry. B) Oxaliplatin (*trans-l*_1R_2R, *trans-d*_1S_2S and *cis*_1R_2S conformers of oxaliplatin in that order from left to right); C) BNP3029 (all *gauche*, all *trans*, *trans/gauche* forms of cyano ligands on BNP3029 in that order from left to right). All distances are in Angstroms (Å) and angles are in degrees.

Optimized geometries of Oxaliplatin

The three isomeric forms of DACH ligand (1,2-diaminocyclohexane; *trans-d*_1S_2S; *trans-l*_1R_2R and *cis*_1R_2S) yield three isomers of oxaliplatin and we optimized all three of them (Figure 2B) [31]. The *trans-l*_1R_2R form of oxaliplatin was more stable than the *trans-d*_1S_2S form of oxaliplatin by 0.28 kcal/mol based upon the solvent-phase optimized geometries and energies after accounting for thermal corrections. There are only a few reported theoretical studies on the geometries and energies of oxaliplatin [9] and data reported indicate that the *trans-d*_1S_2S isomer was more stable than the *trans-l*_1R_2R by 0.30 kcal/mol using gas-phase energies. The optimized geometries of all the three conformers of oxaliplatin are shown in Table 2. As seen in the case of cisplatin, inclusion of solvent (bold numbers in Table 2) led to optimized geometries of oxaliplatin that were in much closer agreement with the experimental values.

Optimized geometries of BNP3029

The structure of BNP3029 is similar to that of cisplatin in that the two carrier ligands (NH_3s) are replaced by two substituted cyano groups or ligands $[(C_6H_5)(CH_2)_3C{\equiv}N]$. These substituted cyano ligands may adopt all *trans*, all *gauche*, or *trans/gauche* arrangements (Figure 2C). The gas-phase optimized energies indicated that the all *gauche* conformer of BNP3029 was more stable than *trans/gauche* conformer by 1.25 kcal/mol, and 1.64 kcal/mol more stable than the all *trans* conformer after accounting for thermal corrections. When these geometries were reoptimized using solvent, a different stability order was observed with the all *trans* conformer appearing more stable than the *trans/gauche* conformer by 1.27 kcal/mol, and the all *gauche* arrangement by 2.89 kcal/mol.

As seen from gas-phase optimized geometries of cisplatin and oxaliplatin, the gas-phase geometries of BNP3029 also showed shortened Pt-Cl bond lengths compared to the Pt-Cl bond lengths from solution-phase optimized geometries (Table 3). Another notable difference was the deviation from linearity in Pt-N-C and N-C-C bond angles using the gas-phase optimized geometries compared to the ones from solvent-phase optimized geometries of BNP3029 (Table 3). A crystal structure for BNP3029 was not available; therefore the calculated geometries of BNP3029 were compared with the related crystal structure, $PtCl_2(N{\equiv}CCH_2CH_3)_2$ [32]. As seen in Table 3, both gas- and solution-phase optimized geometries of BNP3029 are in reasonable agreement with the experimental geometries of $PtCl_2(N{\equiv}CCH_2CH_3)_2$.

Activation energy barriers

In order to elucidate how fast/slow BNP3029 reacts with nucleophiles, as compared to cisplatin, the transition state geometries for the attack of various nucleophiles were optimized at the gas-phase using the above mentioned basis sets and effective core potentials. To evaluate the activation energy barriers, solvent contributions to the gas-phase optimized geometries of the transition state and the

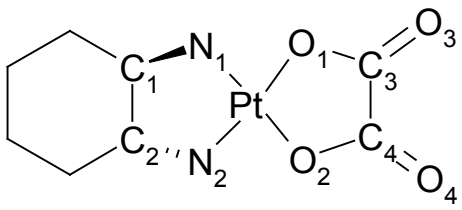

[1]Oxaliplatin_1R_2R [31].

	Pt-N1	Pt-N2	Pt-O1	Pt-O2	C1-C2	C1-N1	C2-N2	O1-C3	O2-C4	C3-O3	C4-O4	C3-C4	N1-Pt-N2	N1-Pt-O1	N2-Pt-O2	O1-Pt-O2	Pt-O2-C4	Pt-O1-C3	O2-C4-C3	O1-C3-C4	O2-C4-O4	O1-C3-O3
1R_2R	**2.034**	**2.034**	**2.029**	**2.029**	**1.521**	**1.487**	**1.487**	**1.299**	**1.299**	**1.223**	**1.223**	**1.544**	**82.9**	**97.6**	**97.6**	**82.0**	**113.5**	**113.5**	**115.5**	**115.5**	**123.9**	**123.9**
	2.067	2.067	1.975	1.975	1.530	1.483	1.482	1.327	1.327	1.203	1.203	1.553	83.0	96.2	96.2	84.6	113.1	113.1	114.6	114.6	123.3	123.3
1S_2S	**2.034**	**2.033**	**2.030**	**2.029**	**1.520**	**1.487**	**1.487**	**1.298**	**1.298**	**1.223**	**1.223**	**1.544**	**82.9**	**97.5**	**97.7**	**81.9**	**113.5**	**113.6**	**115.5**	**115.5**	**123.9**	**123.8**
	2.066	2.067	1.975	1.975	1.529	1.482	1.483	1.327	1.327	1.203	1.203	1.553	83.0	96.2	96.2	84.6	113.1	113.1	114.6	114.6	123.4	123.4
1R_2S	**2.030**	**2.031**	**2.029**	**2.029**	**1.526**	**1.489**	**1.497**	**1.299**	**1.299**	**1.222**	**1.222**	**1.543**	**82.7**	**97.7**	**97.7**	**81.9**	**113.6**	**113.6**	**115.5**	**115.5**	**123.9**	**123/9**
	2.065	2.064	1.975	1.975	1.536	1.489	1.489	1.327	1.327	1.204	1.204	1.553	82.9	96.2	96.3	84.6	113.1	113.1	114.6	114.6	123.4	123.4
Expt[1]	2.040	2.060	2.040	2.010	1.490	1.540	1.540	1.320	1.210	1.190	1.290	1.560	83.8	98.6	96.0	82.5	112.0	141.0	122.0	110.0	124.0	124.0

Table 2: Gas-phase and solution-phase (bold) optimized geometries of oxaliplatin and the comparison of the geometries from experiment. All distances are in Å and angles are in °.

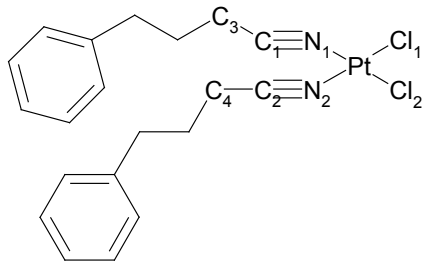

[1]$Pt[N{\equiv}C(C_2H_5)]_2Cl_2$ [32].

	Pt-N1	Pt-N2	Pt-Cl1	Pt-Cl2	N1-C1	N2-C2	C1-C3	C2-C4	N1-Pt-N2	N1-Pt-Cl1	N2-Pt-Cl2	Cl1-Pt-Cl2	Cl2-Pt-N1	Cl1-Pt-N2	Pt-N1-C1	Pt-N2-C2	N1-C1-C3	N2-C2-C4
All *trans*	**1.958**	**1.958**	**2.314**	**2.312**	**1.153**	**1.153**	**1.448**	**1.448**	**90.1**	**89.7**	**89.4**	**90.7**	**179.5**	**179.8**	**178.2**	**179.7**	**179.3**	**178.9**
	1.963	1.963	2.282	2.281	1.154	1.154	1.453	1.453	94.5	86.9	87.2	91.3	178.3	178.5	172.7	173.5	176.7	177.6
gauche/ trans	**1.958**	**1.958**	**2.313**	**2.312**	**1.154**	**1.154**	**1.450**	**1.448**	**90.4**	**89.4**	**89.4**	**90.8**	**179.7**	**179.8**	**179.2**	**179.6**	**179.1**	**179.1**
	1.964	1.960	2.286	2.280	1.154	1.154	1.455	1.453	94.5	86.9	87.4	91.2	178.1	178.6	171.4	174.0	175.5	177.7
All *gauche*	**1.958**	**1.958**	**2.312**	**2.313**	**1.154**	**1.154**	**1.450**	**1.450**	**90.4**	**89.4**	**89.5**	**90.7**	**179.8**	**179.8**	**179.6**	**179.8**	**179.7**	**179.0**
	1.963	1.962	2.286	2.285	1.154	1.154	1.455	1.455	94.9	87.0	87.0	91.2	178.2	178.1	171.5	171.8	175.5	175.8
Expt[1]	1.940	1.980	2.263	2.263	1.200	1.190	1.420	1.440	89.8	89.9	89.6	90.6	179.5	177.0	177.0	175.0	176.0	177.0

Table 3: Gas-phase and solution-phase (bold) optimized geometries of BNP3029 and the comparison of the geometries from experiment[1]. All distances are in Å and angles are in °.

reactants were included. Table 4 provides the activation energy barriers for the attack of nucleophiles on cisplatin and BNP3029 and their monoaquated derivatives. The barriers indicate that the reaction rate may be similar for the attack of water on cisplatin and BNP3029; the reaction rate for the attack of guanine or adenine on monoaquated BNP3029 is slower compared to an attack by the same nucleophiles on monoaqauted cisplatin; and the reaction rate may be similar for the attack of thiol or thiolate on monoaquated cisplatin and monoaquated BNP3029 (energy barriers and the transition state (TS) geometries are explained in detail below).

Activation energy barriers for the aquation of Cisplatin and BNP3029 (eq. 1) and the TS geometries for aquation (1a and 3a)

Several computational studies identify the transition state for the nucleophilic attack of water on cisplatin as trigonal bipyramidal (TBP) geometry with the incoming water and the outgoing chloride ion along with the one of the ammines occupying the equatorial plane (Figure 3A, 1a) [11-14]. A similar TBP transition state geometry was also found for the nucleophilic attack of water on BNP3029 (Figure 3B, 3a). The activation free energies (for details see activation free energy barrier calculation section) are given in Table 4. The computed activation free energy barrier for the aquation of cisplatin was 2-4 kcal/mol higher compared to the experimental barriers. The barriers from Table 4 indicate that the activation free energy barrier is slightly higher for 3a compared to 1a. The magnitude of the difference, which is within the typical margin of the computational error, may indicate that the reaction rate going through this transition state and forming the monoaquated species may be similar for cisplatin and BNP3029. The TBP geometry for the TS attack of water on cisplatin (1a) and BNP3029 (3a) and the geometric parameters are given in Figure 3.

The geometry of 1a (Figure 3C), but not 3a, was optimized using

Nucleophile	Cisplatin	BNP3029
OH_2	27.7 **23.8**[b], **24.1**[c],**24.3 ± 1.5**[d]	28.6
Guanine	21.1 **23.4**[e]	24.0
Adenine	30.3	34.5
SCH_3^{-1}	14.9	15.7
$SHCH_3$	27.8	29.3

[a]Thermal corrections to the free energies were obtained from frequency calculations at 25 ºC and 1 atm.
When comparing the calculated activation energy barriers with experimental data, the calculated energy barriers were corrected for liquid-phase concentrations of 1 mol/L by subtracting 1.9 kcal/mol from the calculated activation energy barriers.
[b]See reference 34.
[c]See reference 33.
[d]See reference 12.
[e]See reference 35.

Table 4: Activation free energies[a] for the nucleophilic attack of water on cisplatin and BNP3029; or for the nucleophilic attack on monoaquated cisplatin or BNP3029 by guanine, adenine, thiolate and thiol. Bold numbers refer to the experimental activation free energies.

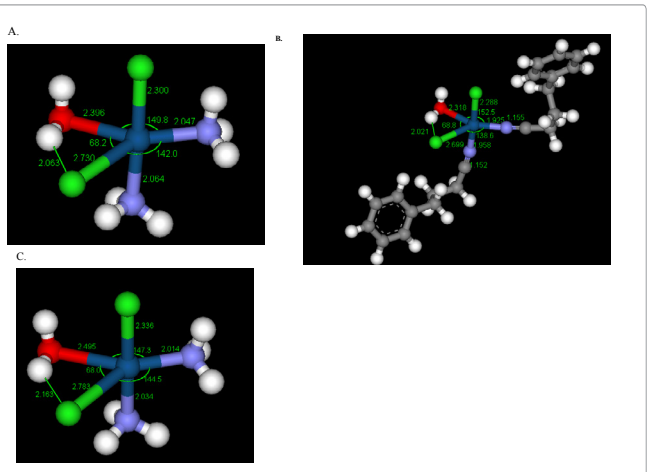

Figure 3: Optimized transition state geometry for the aquation of A) Cisplatin from gas-phase: $Pt(NH_3)_2Cl_2(OH_2)$ (**1a**). B) BNP3029 from gas-phase: $Pt[N{\equiv}C(CH_2)_3(C_6H_5)]_2Cl_2(OH_2)$ (**3a**). All distances are in Angstroms (Å) and angles are in degrees. C) Cisplatin from solution-phase: $Pt(NH_3)_2Cl_2(OH_2)$ (**1a**)..

solvent. Optimized geometries of cisplatin (1, gas- and solution- phase, Table 1) indicated that the inclusion of solvent resulted in increased Pt-Cl bond lengths. A similar trend in Pt-Cl bond lengths was obtained with the inclusion of solvent during the optimization of 1a compared to the gas-phase geometries (Pt-Cl_{eq} bond length in gas-phase: 2.730 Å and solution-phase: 2.783 Å). Inclusion of solvent also resulted in the increase of the Pt-OH_2 bond lengths (gas-phase: 2.396 Å and solution-phase: 2.495 Å) leading to a late TS (identified as having a geometry with long Pt-Cl (leaving) and long Pt-OH_2 (incoming) bond lengths).

The equatorial bond lengths of Pt-Cl (2.699 Å) and Pt-OH_2 (2.318 Å) in 3a (gas-phase) compared to the equatorial bond lengths of Pt-Cl (2.730 Å) and Pt-OH_2 (2.396 Å) in 1a (gas-phase) were indicative of an early transition state for 3a (identified as having a geometry with short Pt-Cl (leaving) and short Pt-OH_2 (incoming) bond lengths). The Cyano$_{eq}$-Pt-O$_{eq}$ bond angle (152.5º) was larger for 3a compared to that in 1a (149.8º), leading to a shorter OH_2-H---Cl distance in 3a (2.021 Å) compared to that in 1a (2.063 Å). Since O$_{eq}$-Pt-Cl$_{eq}$ bond angles were similar in 1a and 3a, the Cyano$_{eq}$-Pt-Cl$_{eq}$ bond angle in 3a (138.6º) became shorter than the corresponding value in 1a (142.0º).

Activation energy barriers for the attack of DNA bases (guanine, eq. 2 and adenine, eq. 3) on monoaquated cisplatin and monoaquated BNP3029 and the TS geometries (1b, 3b; and 1c, 3c)

Nucleophilic attack by DNA bases (guanine or adenine) on monoaquated cisplatin or monoaquated BNP3029 also resulted in a transition state geometry similar to 1a and 3a. The incoming DNA bases and the outgoing water, along with one of the ammines, occupy the equatorial plane. The computed activation energy barrier for the attack of guanine on monoaquated cisplatin was 2.3 kcal/mol lower compared to the experimental barrier. As seen in Table 4, the barrier for the attack of guanine on monoaquated cisplatin is lower than that for monoaquated BNP3029, indicating a faster reaction of guanine with monoaquated cisplatin (equation 2). The activation free energy barrier for the attack of adenine on monoaquated cisplatin is higher compared to that of the barrier obtained for the attack of guanine on monoaquated cisplatin (Table 4). This observation is in accord with the

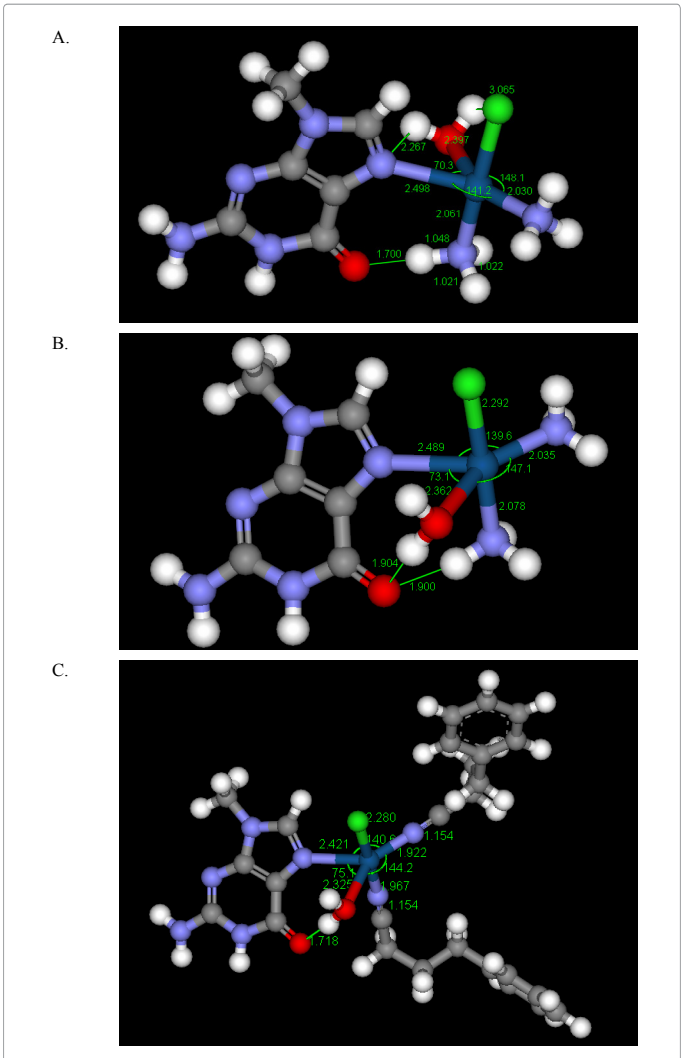

Figure 4: Optimized transition state geometry for the guanine attack on A) monoaquated cisplatin from gas-phase: $Pt(NH_3)_2Cl(OH_2)$(guanine) (**1b**); B) monoaquated cisplatin from gas-phase: $Pt(NH_3)_2Cl(OH_2)$(guanine) (**1b**); C) monoaquated BNP3029 from gas-phase: $Pt[N{\equiv}C(CH_2)_3(C_6H_5)]_2Cl(OH_2)$ (guanine) (**3b**). All distances are in Angstroms (Å) and angles are in degrees.

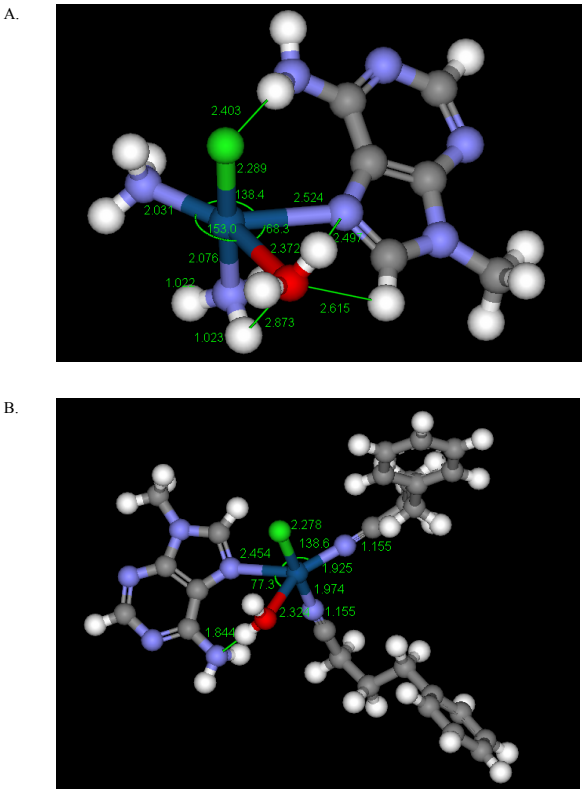

Figure 5: Optimized transition state geometry for the adenine attack on A) monoaquated cisplatin from gas-phase: $Pt(NH_3)_2Cl(OH_2)$(adenine) (**1c**); B) monoaquated BNP3029 from gas-phase: $Pt[N{\equiv}C(CH_2)_3(C_6H_5)]_2Cl(OH_2)$ (adenine) (**3c**). All distances are in Angstroms (Å) and angles are in degrees.

data from previous studies indicating that guanine was the preferred site of attack by monoaquated cisplatin followed by adenine. As seen with the nucleophilic attack by guanine and adenine on monoaquated cisplatin, the reaction rate for adenine with monoaquated BNP3029 is slower compared to the reaction rate of guanine with monoaquated BNP3029 (Table 4).

The TS geometry for the attack of guanine on monoaquated cisplatin (1b) resembles a TBP with the leaving OH_2, incoming guanine, and one of the NH_3 forming the equatorial plane, and the other NH_3 and Cl^- occupying the axial positions (Figure 4A). One of the hydrogens from the axial NH_3 is in hydrogen-bond contact with the O6 of guanine (1.700 Å). As a consequence, the hydrogen's distance with ammonia N increases to 1.048 Å compared to other two N-H distances which were 1.021 Å and 1.022 Å. A second TS geometry for 1b (similar 1b geometry was obtained by Costa et al. [18]) is shown in Figure 4B. This TS geometry resulted in a slightly higher activation free energy barrier compared to the TS geometry presented in Figure 4A. In Figure 4B, the outgoing OH_2 is in hydrogen-bond contact with the O6 atom of the incoming guanine (1.904 Å). Also, the O6 atom of the incoming guanine is in hydrogen-bond contact with the axial NH_3 hydrogen (1.900 Å) as seen in Figure 4A. The equatorial Pt-N7 and Pt-O bond lengths are longer in Figure 4A (2.498 Å and 2.397 Å) than in Figure 4B (2.489 Å and 2.362 Å). As a result, $N7_{eq}$-Pt-O_{eq} bond angle (73.1°) in Figure 4B is slightly larger than that in Figure 4A (70.3°).

The TS geometry for the attack of guanine on monoaquated BNP3029 (Figure 4C, 3b) exhibited similar TBP geometry with the leaving OH_2, incoming guanine, and one of the cyano ligands forming the equatorial plane, and the other cyano ligand and Cl^- occupying the axial positions. Since O6 of guanine cannot hydrogen-bond with the cyano ligand, the O6 of guanine forms hydrogen-bonds with the equatorial bound OH_2 (1.718 Å) hydrogens. This TS geometry of 3b is similar to the TS geometry obtained for the attack of guanine on monoaquated cisplatin by Costa et al. (Figure 4B) [18]. The $Cyano_{eq}$-Pt-O_{eq} bond angle (144.2°) is smaller in 3b compared to the value observed in 1b (148.1°, Figure 4A). Correspondingly, the $N7_{eq}$-Pt-O_{eq} bond angle becomes wider in 3b (75.1°, Figure 4C) versus 1b (70.3°, Figure 4A).

The main features of the transition state geometry for the attack of adenine on monoaquated cisplatin (Figure 5A, 1c) are the NH_2---Cl contact between C6-NH_2 of Adenine and the axial Cl^- (2.403 Å); the OH_2-O hydrogen-bond contact with the axial NH_3-H (2.873 Å); the OH_2-O O---C-H contact with the C8-H (2.615 Å) of adenine; the hydrogen-bond contact between N7(adenine)---H-OH_2 (2.497 Å); and the equatorial NH_3-H---Cl contact of 2.525 Å. Since both OH_2 and equatorial NH_3 are involved in hydrogen-bond interactions, we noticed an increase of the $NH_{3(eq)}$-Pt-$OH_{2(eq)}$ bond angle from 148.1° in 1b to 153.0° in 1c. Accordingly, the $OH_{2(eq)}$-Pt-$N7_{eq}$ bond angle (adenine in the equatorial position) shortens by 2° from the value in 1b.

The transition state geometry for the attack of adenine on monoaquated BNP3029 (Figure 5B, 3c) shows hydrogen-bond contact between OH_2-H and the adenine C6-NH_2 (1.844 Å), OH_2-H---Cl (axial) contact of 2.745 Å, and a concomitant decrease in the $Cyano_{(eq)}$-Pt-$N7_{(adenine, eq)}$ bond angle from 140.6° in 3b to 138.6° in 3c. Accordingly, $OH_{2(eq)}$-Pt-$N7_{(adenine, eq)}$ increases by 2° in 3c compared to the value in 3b.

Activation energy barriers for the attack of thiol (eq. 4) and thiolate (eq. 5) on monoaquated cisplatin and monoaquated BNP3029 and the TS geometries (1d, 3d; and 1e, 3e)

Thiol-containing biomolecules such as glutathione are known to inactivate cisplatin. Since pH is a function of the existing micro environment, nucleophilic attacks on monoaquated cisplatin and monoaquated BNP3029 by thiol ($HSCH_3$) and thiolate ($^-SCH_3$) forms of the biological equivalent of cysteine were studied. The nucleophilic attack by thiol or thiolate on monoaquated cisplatin or monoaquated BNP3029 resulted in a TBP transition state geometry. The incoming thiol or thiolate and the outgoing water, along with one of the ammines, occupy the equatorial plane. As seen in Table 4, the barrier for the attack of thiol on monoaquated cisplatin is slightly lower than the barrier seen with monoaquated BNP3029, indicating a faster reaction of thiol with monoaquated cisplatin, whereas the barriers for the thiolate attack on monoaquated cisplatin and monoaquated BNP3029 are similar.

The TS geometries for the attack of thiol on monoaquated cisplatin (1d) and monoaqauted BNP3029 (3d) resemble a TBP arrangement with the leaving OH_2, incoming thiol, and one of the ammine (substituted cyano group) forming the equatorial plane, and the other ammine (substituted cyano group) and Cl^- occupying the axial positions are shown in Figure 6. In the TS geometry of 3d (Figure 6B), the hydrogen on thiol is in hydrogen-bond contact with the O of OH_2 (2.673 Å), and the H on OH_2 is in contact with the axial Cl^- (2.497 Å). The above two contacts are also noticed in the TS geometry of 1d (Figure 6A, 2.736 Å and 2.618 Å respectively). The N_{eq}-Pt-O_{eq} bond angle is similar in 1d (151.9°) and 3d (152.8°). Additionally, the S_{eq}-Pt-O_{eq} bond angle is wider in both 1d (73.6°) and 3d (74.5°) and as a consequence the N_{eq}-Pt-S_{eq} bond angle is shorter in both 1d (133.7°) and 3d (132.2°).

The transition state geometries for the attack of thiolate on monoaquated cisplatin (1e) and monoaquated BNP3029 (3e) also

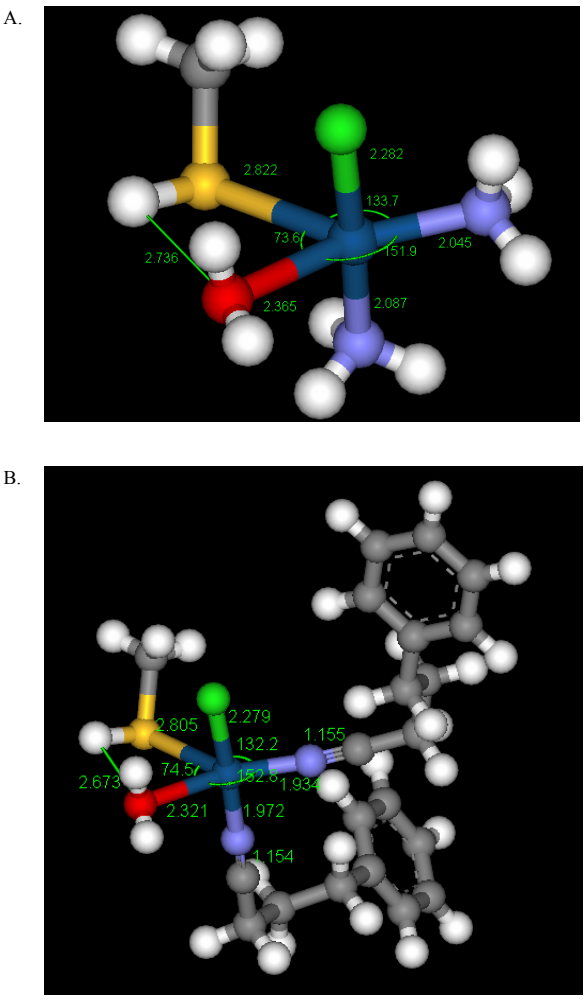

Figure 6: Optimized transition state geometry for the thiol attack on A) monoaquated cisplatin: $Pt(NH_3)_2Cl(OH_2)(SHCH_3)$ (**1d**); B) monoaquated BNP3029: $Pt[N{\equiv}C(CH_2)_3(C_6H_5)]_2Cl(OH_2)(SHCH_3)$ (**3d**). All distances are in Angstroms (Å) and angles are in degrees.

resemble the TBP arrangement with the leaving OH_2, incoming thiolate, and one of the ammines (substituted cyano group) forming the equatorial plane, and the other ammine (substituted cyano group) and Cl^- occupying the axial positions (Figure 7). In the TS geometry of 1e (Figure 7A), one of the hydrogens on OH_2 is in contact with the thiol-S (2.036 Å), and the other hydrogen is in contact with the axial Cl^- (2.715 Å). The above two contacts are also noticed in the TS geometry of 3e (Figure 7B, 1.970 Å and 2.652 Å respectively). The S_{eq}-Pt-O_{eq} bond angle is similar in 1e (67.1°) and 3e (68.8°). Additionally, the N_{eq}-Pt-O_{eq} bond angle is wider in 3e (161.8°) compared to the one in 1e (157.6°), and as a consequence the N_{eq}-Pt-S_{eq} bond angle is shorter in 3e (130.1°) compared to the value in 1e (135.3°).

Cytotoxicity data for cisplatin, oxaliplatin and BNP3029 in wild-type and resistant cell lines

In order to assess the efficacy of the novel substituted cyano ligand-based platinum analogue, cytotoxicity of BNP3029 in a variety of human cancer cell lines was determined with cisplatin and oxaliplatin included as comparators. For comparison purposes, we also included cisplatin and oxaliplatin in the IC50 evaluations. As seen in Table 5, in the wild-type cell lines, including A2780 (ovarian cancer), MCF7 (breast cancer), NCI-H23 (non-small cell lung cancer), NCI-H838 (non-small cell lung cancer), CAMA-1 (breast cancer), SW480 (colon cancer), and HCT8 (colon cancer), BNP3029 consistently showed superior IC_{50} activity compared to cisplatin and oxaliplatin (except with respect to the GLC (small cell lung cancer) cell line, where BNP3029 showed comparable activity). Also, BNP3029 showed very promising activity in resistant cell types for A2780 (CP3 and C25), MCF7 (MR, ADR, OxR) and HCT8 (CisR), with better resistance factors (resistance factors were obtained by dividing the IC50 in resistant cell type by the IC50 in wild-type cell line).

Discussion

Since the discovery of cisplatin's antitumor properties, many platinum analogues have been made and evaluated in clinical trials, yet very few have been approved for use in patients. Several studies have focused on understanding the activation energy barriers for the attack of nucleophiles on cisplatin or the monoaquated cisplatin to understand the platinum analogue's reactivity.

The optimized geometries of cisplatin, oxaliplatin, and BNP3029

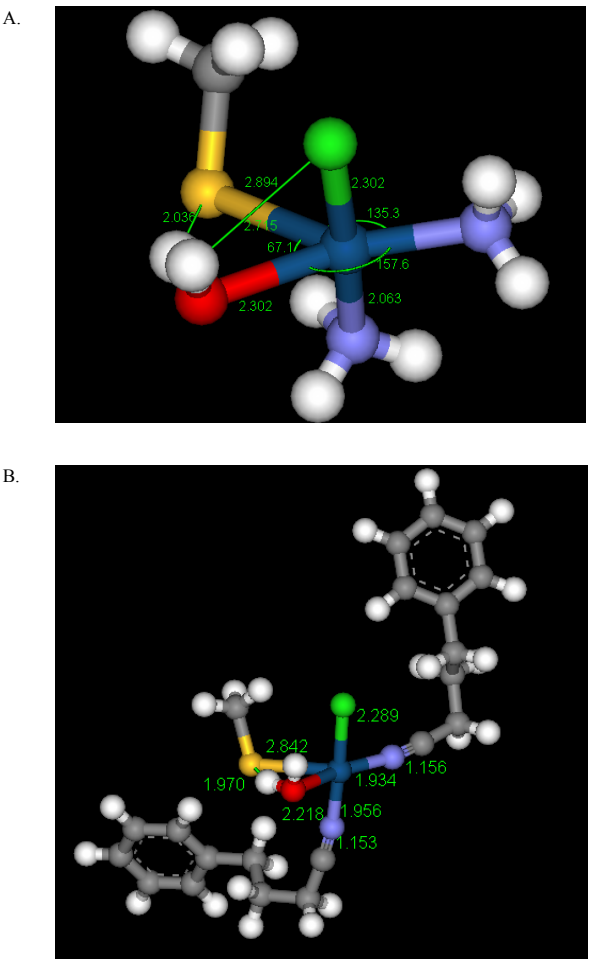

Figure 7: Optimized transition state geometry for the thiolate attack on A) monoaquated cisplatin: $Pt(NH_3)_2Cl(OH_2)(SCH_3)$ (**1e**); B) monoaquated BNP3029: $Pt[N{\equiv}C(CH_2)_3(C_6H_5)]_2Cl(OH_2)(SCH_3)$ (**3e**). All distances are in Angstroms (Å) and angles are in degrees.

	IC50 (μM)														
	A2780			MCF7				GLC		NCI-H23	NCI-H838	CAMA-1	SW480	HCT8	HCT8
Drug	WT	CP3	C25	WT	MR	ADR	OxR	WT	ADR	WT	WT	WT	WT	WT	CisR
CDDP	6.4	77.3	30.8	14.2	39.7	14.8	19.3	4.1	7.0	4.3	12.5	12.3	13.5	31.9	126.5
Oxaliplatin	4.0	23.4	43.7	20.4	47.7	32.1	131.5	3.7*	9.6*	13.9	>100	36.4	36.1		
BNP3029	3.8	6.5	4.8	2.96	7.08	1.92	2.51	4.3	5.7	2.4	2.2	2.0	1.9	2.73	2.65

Table 5: IC_{50} (μM) values for cisplatin, oxaliplatin and BNP3029 using a variety of wild-type (WT) and drug-resistant cell lines.
A2780/WT: human wild type ovarian cancer cell line; A270/CP3 is A2780 with cisplatin resistance cell line; A2780/C25 is A2780 with oxaliplatin resistance cell line; MCF7/WT: human wild type breast cancer cell line; MCF7/MR is MCF7 with mitoxantrone resistance cell line; MCF7/ADR is MCF7 with adriamycin resistance cell line; MCF7/OxR is MCF7 with oxaliplatin resistance cell line; GLC/WT: human wild type small cell lung cancer; GLC/ADR is humanGLC with adriamycin resistance cell line; NCI-H23/WT: human wild type non-small cell lung cancer (adenocarcinoma); NCI-H838/WT: human wild type non-small cell lung cancer (adenocarcinoma); CAMA-1/WT: human wild type breast cancer (adenocarcinoma); SW480/WT: human wild type colorectal cancer (adenocarcinoma); HCT8/WT: human wild type colorectal cancer (adenocarcinoma); HCT8/CisR: humanHCT8 with cisplatin resistance cell line.

(novel substituted cyano ligand-based platinum analogue) employing the most current basis set and potentials for platinum resulted in good agreement with the experimental data, where available, with the inclusion of solvent providing a closer agreement. Studies described herein compared the reactivity of cisplatin and BNP3029 or their monoaquated species in their ability to react with various nucleophiles. Again, the computed activation free energy barriers were in reasonable agreement with experimental data for cisplatin. BNP3029 showed increased activation energy barriers for some nucleophiles such as guanine and adenine, indicating a slower reactivity with these nucleophiles compared to cisplatin. The reactivity of BNP3029 with other nucleophiles such as water or thiolate/thiol may be similar compared to cisplatin's reactivity with these nucleophiles (the barriers for BNP3029 were slightly higher compared to the barriers with cisplatin). With no involvement of either NH_3s or substituted cyano ligand (axial or equatorial), the transition state geometries (from gas-phase) for the aquation of cisplatin or BNP3029 indicate that only the leaving Cl and the incoming OH_2 are involved in leading to early (in case of BNP3029, Figure 3C) or slightly late (in case of cisplatin, Figure 3A) TS, thereby leading to similar barriers (albeit slightly higher in the case of BNP3029) for aquation.

The guanine nucleophile participates in stabilizing interactions with the axial NH_3 in the case of monoaquated cisplatin (Figure 4A). However, such interactions are not possible with monoaquated BNP3029 due to the lack of hydrogens on substituted cyano ligands (Figure 4C) which may lead to higher barriers for the reaction of guanine with monoaquated BNP3029. In the reaction of adenine with monoaquated cisplatin, stabilizing interactions between OH_2 and axial NH_3, and between C6-NH_2 and axial Cl (Figure 5A), lead to a decreased barrier for adenine reacting with monoaquated cisplatin compared to a similar reaction of adenine with monoaquated BNP3029, due to the lack of hydrogens on the substituted cyano ligands.

Again, with no involvement of either NH_3s or substituted cyano ligand (axial or equatorial), the transition state geometries (gas-phase) for the reaction of thiol/thiolate with monoaquated cisplatin or monoaquated BNP3029 indicate that only the leaving OH_2 and the incoming thiol/thiolate are involved in leading to an early (in the case of BNP3029, Figure 6B and 7B) or slightly late (in the case of cisplatin, Figure 6A and 7A) TS, thereby leading to similar barriers (albeit slightly higher in the case of BNP3029) for thiol/thiolate attack. Our computational calculations indicated novel properties in silico for BNP3029 and importantly, in vitro IC50 evaluations of BNP3029 in comparison to cisplatin and oxaliplatin also indicated superior IC50 data for BNP3029 (Table 5) in a variety of wild-type and resistant human cancer cell lines.

Conclusions

Ab initio geometry optimizations (gas- and solution-phase) using the recently published energy-consistent pseudo-potentials and correlation consistent basis set for platinum and cc-pVDZ basis set on ligand atoms of cisplatin, oxaliplatin, and BNP3029 (a substituted cyano ligand-based platinum analogue) within the density functional formalism were conducted. The optimized geometries compared very well with the available experimental data for cisplatin and oxaliplatin. Transition state geometries for the nucleophilic attack of water on cisplatin and BNP3029, as well as the TS geometries for the nucleophilic attacks of guanine, adenine, thiol and thiolate on their monoaquated derivatives were also determined. Our computed data indicate that in terms of water attack both cisplatin and BNP3029 have similar activation energy barriers; the barrier for the attack of guanine and adenine was increased for monoaquated BNP3029 compared to that of monoaquated cisplatin. However, the barriers for a thiol/thiolate attack on monoaquated cisplatin and monoaquated BNP3029 were similar.

In vitro, BNP3029 had more potent activity in a variety of human cancer cell lines compared to cisplatin and oxaliplatin. BNP3029 also had potent activity in cell lines traditionally resistant to cisplatin and oxaliplatin.

Acknowledgement

NCI-H23 and NCI-H838 were developed in the laboratory of Dr. Herbert Oie and were used pursuant to a license obtained from the Public Health Service/National Institutes of Health. We thank Dr. Yusef Rustum, Dr. W. Dalton, Dr. EGE de Vries and Dr. C. Meijer for gifts of other cell lines described in the materials and methods. We thank Joe Zdanowicz for preliminary work in developing proprietary platinum resistant cell lines.

References

1. Reed E (2008) In: DeVita, Jr. VT, Lawrence TS, Rosenberg SA (eds) Cancer, Principles & Practice of Oncology, 8th edn. Lippincott Williams & Wilkins, Philadelphia 419-426.
2. Dhar S, Lippard SJ (2011) Current Status and Mechanism of Action of Platinum-Based Anticancer Drugs, In: Alessio E (ed) Bioinorganic Medicinal Chemistry, Wiley-VCH Verlag GmbH & Co. KGaA, Weinheim, Germany, Chapter 3: 79-95.
3. Wheate NJ, Walker S, Craig GE, Oun R (2010) The status of platinum anticancer drugs in the clinic and in clinical trials. Dalton Trans 39: 8113-8127.
4. Raymond E, Chaney SG, Taamma A, Cvitkovic E (1998) Oxaliplatin: a review of preclinical and clinical studies. Ann Oncol 9: 1053-1071.
5. Wang X (2010) Fresh platinum complexes with promising antitumor activity. Anticancer Agents Med Chem 10: 396-411.
6. Bhargava A, Vaishampayan UN (2009) Satraplatin: leading the new generation of oral platinum agents. Expert Opin Investig Drugs 18: 1787-1797.
7. Chen X, Petluru P, Huang Q, Narkunan K, Hausheer F (2010) Platinum Analogs with Bis-Nitrile-Containing Ligands US Patent No. 7,777,060.
8. Gao H, Xia F, Huang C-J, Lin K (2011) Density functional theory calculations on the molecular structures and vibration spectra of platinum(II) antitumor drugs. Spectrochim Acta A Mol Biomol Spectrosc 78:1234-1239.

9. Tyagi P, Gahlot P, Kakkar R (2008) Structural aspects of the anti-cancer drug oxaliplatin: A combined theoretical and experimental study. Polyhedron 27: 3567-3574.

10. Pavankumar PNV, Seetharamulu P, Yao S, Saxe JD, Reddy DG, et al. (1999) Comprehensive Ab Initio quantum mechanical and molecular orbital (MO) analysis of cisplatin: Structure, Bonding, Charge Density, and Vibrational Frequencies. J Comput Chem 20:365-382.

11. Burda JV, Zeizinger M, Sponer J, Leszczynski J (2000) Hydration of cis- and trans-platin: A pseudopotential treatment in the frame of a G3-type theory for platinum complexes. J Chem Phys 113: 2224-2232.

12. Robertazzi A, Platts JA (2004) Hydrogen bonding, solvation, and hydrolysis of cisplatin: a theoretical study. J Comput Chem 25: 1060-1067.

13. Lau JK-C, Deubel DV (2006) Hydrolysis of the anticancer drug cisplatin: Pitfalls in the interpretation of quantum chemical calculations. J Chem Theory Comput 2:103-106.

14. Zhang Y, Guo Z, You XZ (2001) Hydrolysis theory for cisplatin and its analogues based on density functional studies. J Am Chem Soc 123: 9378-9387.

15. Baik MH, Friesner RA, Lippard SJ (2003) Theoretical study of cisplatin binding to purine bases: why does cisplatin prefer guanine over adenine?J Am Chem Soc 125: 14082-14092.

16. Burda JV, Leszczynski J (2003) How strong can the bend be on a DNA helix from cisplatin? DFT and MP2 quantum chemical calculations of cisplatin-bridged DNA purine bases. In org Chem 42: 7162-7172.

17. Bhattacharyya D, Ramachandran S, Sharma S, Pathmasiri W, King CL, et al. (2011) Flanking bases influence the nature of DNA distortion by platinum ,2-intrastrand (GG) cross-links. PLoS One 6: e23582.

18. Costa LAS, Hambley TW, Rocha WR, De Almeida WB, Dos Santos HF (2006) Kinetics and structural aspects of the cisplatin interactions with guanine: A quantum mechanical description. Int J Quantum Chem 106: 2129-2144.

19. Chojnacki H, Kuduk-Jaworska J, Jaroszewicz I, Jaski JJ (2009) Insilico approach to cisplatin toxicity. Quantum chemical studies on platinum(II)-cysteine systems. J Mol Model 15: 659-664.

20. Da Silva VJ, Costa LAS, Dos Santos HF (2008) Ab Initio reaction path for cisplatin interaction with L-cysteine and L-methionine. Int J Quantum Chem 108: 401-414.

21. Zimmermann T, Burda JV (2010) Reactions of cisplatin with cysteine and methionine at constant pH; a computational study.Dalton Trans 39: 1295-1301.

22. Gaussian , Frisch MJ, Trucks GW, Schlegel HB, Scuseria GE, et al. (2004) Gaussian, Inc. Wallingford, CT.

23. Skehan P, Storeng R, Scudiero D, Monks A, McMahon J, et al. (1990) New colorimetric cytotoxicity assay for anticancer-drug screening. J Natl Cancer Inst 82: 1107-1112.

24. Cramer CJ,Truhlar DG (2009) Density functional theory for transition metals and transition metal chemistry. Phys Chem Chem Phys 11: 10757-10816.

25. Adamo C, Barone V (1998) Exchange functionals with improved long-range behavior and adiabatic connection methods without adjustable parameters: The mPW and mPW1PW models. J Chem Phys 108: 664-675.

26. Woon DE, Dunning TH (1993) Gaussian basis sets for use in correlated molecular calculations. III. The atoms aluminum through argon. J Chem Phys 98: 1358-1371.

27. Figgen D, Peterson KA, Dolg M, Stoll H (2009) Energy-consistent pseudo potentials and correlation consistent basis sets for the 5d elements Hf-Pt. J Chem Phys 130: 164108.

28. Kelly CP, Cramer CJ, Truhlar DG (2006) Aqueous solvation free energies of ions and ion-water clusters based on an accurate value for the absolute aqueous solvation free energy of the proton.J Phys Chem B 110: 16066-16081.

29. Cances E, Mennucci B, Tomasi J (1997) A new integral equation formalism for the polarizable continuum model.: Theoretical background and applications to isotropic and anisotropic dielectrics. J Chem Phys 107: 3032-3031.

30. Milburn GHW, Truter MR (1966) The crystal structures of cis- and trans-dichlorodiammineplatinum(II). J Chem Soc (A) 1609-1615.

31. Bruck MA, Bau R, Noji M, Inagaki K, Kidani Y (1984) The crystal structures and absolute configurations of the anti-tumor complexes Pt(oxalato)(1R,2R-cyclohexanediamine) and Pt(malonato)(1R,2R-cyclohexanediamine). In org Chim Acta 92: 279-284.

32. Svensson P, Lovqvist K, Yu Kukushkin V, Oskarsson A (1995) Thermal cis to trans isomerization of [PtCl2(C2H5CN)2] and crystal structures of the cis- and trans-isomers. Acta ChimScand 49:72-75

33. Perumareddi JR, Adamson AW (1968) Photochemistry of complex ions. V. Photochemistry of some square-planar platinum(II) complexes. J Phys Chem 72:414-420.

34. Coe JS (1974) MTP Int Rev Sci, Inorg Chem Ser 2: 45.

35. Bancroft DP, Lepre CA, Lippard SJ (1990) Platinum-195 NMR kinetic and mechanistic studies of cis- and trans-diamminedichloroplatinum(II) binding to DNA. J Am Chem Soc 112:6860-6871.